JOURNAL OF AIRCRAFT
Vol. 43, No. 5, September–October 2006

Longitudinal Dynamics of a Perching Aircraft

Adam M. Wickenheiser* and Ephrahim Garcia†
Cornell University, Ithaca, New York 14850

DOI: 10.2514/1.20197

This paper introduces a morphing aircraft concept whose purpose is to demonstrate a new bioinspired flight capability: perching. Perching is a maneuver that uses primarily aerodynamics, as opposed to thrust generation, to achieve a vertical or short landing. The flight vehicle that will accomplish this is described herein with particular emphasis on its addition levels of actuation beyond the traditional aircraft control surfaces. The dynamics of this aircraft are examined with respect to changing vehicle configuration and flight condition. The analysis methodologies include an analytical and empirical aerodynamic analysis, trim and stability analyses, and flight simulation. For this study, the aircraft's motions are limited to the longitudinal plane only. Specifically, cruise and the perching maneuver are examined, and comparisons are drawn between maneuvers involving vehicle reconfiguration and those that do not.

Nomenclature

D	=	aircraft drag force
f_x, X	=	x-component of external force
f_z, Z	=	z-component of external force
$\mathbf{f}$	=	external force vector
g	=	gravity magnitude
$\mathbf{g}$	=	gravity vector
I_y	=	principal moment of inertia about y-axis
$\mathbf{I}$	=	moment of inertia matrix
L	=	aircraft lift force
M	=	aircraft pitch moment
m	=	aircraft mass
m_y	=	y-component of external moment
$\mathbf{m}$	=	external moment vector
q	=	pitch rate
$\mathbf{q}$	=	quaternion
T	=	thrust magnitude
$\mathbf{T}$	=	transformation matrix from body- to earth-coordinates
u	=	x-component of aircraft velocity
V	=	aircraft velocity magnitude
v	=	y-component of aircraft velocity
$\mathbf{v}$	=	aircraft velocity vector (body coordinates)
w	=	z-component of aircraft velocity
x	=	forward direction
$\mathbf{x}$	=	aircraft position vector (inertial coordinates)
y	=	sidereal direction
z	=	vertical direction
α	=	angle of attack
β	=	sideslip angle
δ_a	=	aileron deflection angle
δ_e	=	elevator or symmetric ruddervator deflection angle
θ	=	pitch angle
θ_b	=	boom angle with respect to fuselage
θ_t	=	tail angle with respect to boom
Θ_0	=	trim pitch angle
ι	=	wing incidence angle
ϕ	=	roll angle
ψ	=	yaw angle
$\boldsymbol{\omega}$	=	aircraft angular velocity vector
$\boldsymbol{\omega}^{\times}$	=	skew-symmetric cross product matrix of $\boldsymbol{\omega}$

Received 22 September 2005; accepted for publication 5 January 2006.

*Graduate Student, Sibley School of Mechanical & Aerospace Engineering, 226 Upson Hall, AIAA Student Member.

†Associate Professor, Sibley School of Mechanical & Aerospace Engineering, 224 Upson Hall, AIAA Member.

Introduction

ONE of the major goals of the morphing aircraft program is the enabling of new flight capabilities and missions [1–3]. With additional levels of sensing and actuation, morphing aircraft are able to mimic more closely the capabilities of man's inspiration for flight: birds. The gross extent to which birds morph their bodies allow them to perform maneuvers irreproducible by conventional aircraft; one such avian maneuver is perching. Perching can be described as a high angle-of-attack approach with the purpose of using high-drag, separated flow for braking, followed by a vertical or very short landing [4]. This maneuver is based off of several avian landing techniques, including maximizing drag by flaring the wings and tail, and diving under the intended landing site and then pulling up into a climb to reduce speed. Although vertical landings have been accomplished by rotary and V/STOL aircraft, it is desired to perch using primarily aerodynamics, with little input from thrust-generating devices. This will alleviate the need for the heavy thrust generators required to land vertically, which are not compatible with long endurance aircraft systems. Thus, perching will be especially useful for small, efficient reconnaissance aircraft, for example, whose thrust-to-weight ratios might be on the order of 1/10.

This paper presents a concept for a perching aircraft and an analysis of its longitudinal dynamics. This concept is based on the aerial regional-scale environmental survey (ARES) Mars scout craft, an aircraft designed to unfold from a Viking derivative aeroshell and fly for approximately 70 min over a Martian landscape, collecting data on atmospheric chemistry, geology, and crustal magnetism [5]. The idea to try to perch a similar airframe grew from the challenge to save the ARES scout from a high-speed crash landing at the end of its mission by using drag to slow it down enough to land with its instruments intact. It is desired to perform the perching maneuver without complicating the aircraft system unnecessarily and by adding the fewest number of additional actuators. The original ARES craft features a blended-wing body with folding tail boom, tail surfaces, and wings, shown in Fig. 1. The inverted V-tail features two ruddervators which combine the functionality of a rudder and an elevator. To add perching capabilities, actuators are incorporated into the tail degrees of freedom and variable incidence is added to the folding wing sections. These additional degrees of actuation in the perching flight vehicle, dubbed the ARES-C, are shown in Fig. 2.

The level of geometric reconfigurability required to recreate the perching maneuver in a man-made aircraft falls far outside the bounds of conventional aircraft designs. To maintain stability and controllability at the high angles of attack required for aerodynamic braking, the aircraft's wings are rotated to a negative incidence angle

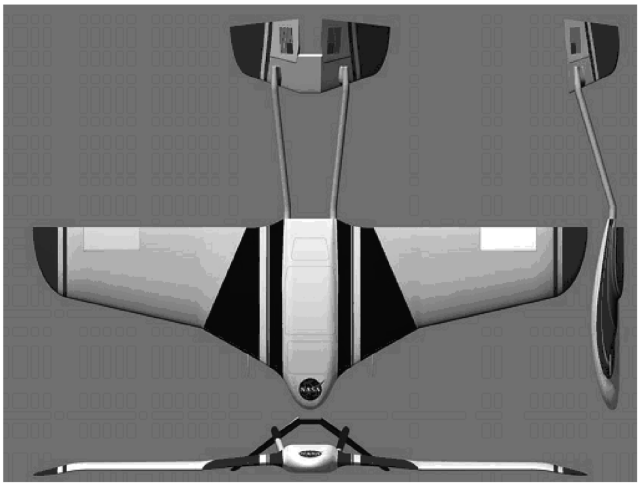

Fig. 1 The ARES Mars scout [13].

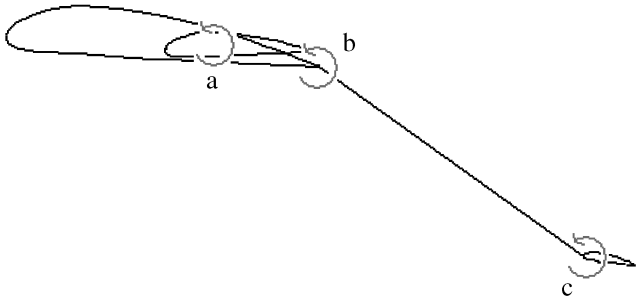

Fig. 2 Morphing degrees of freedom: a) variable wing incidence, b) tail boom rotation, and c) horizontal stabilizer rotation.

to moderate their angle of attack with respect to the oncoming air as the body's angle of attack increases past stall. Additionally, the tail is rotated down and out of the resulting unsteady wake of the body and the horizontal stabilizer is also actuated to remain in the linear angle-of-attack range as the tail boom rotates. These actuations keep the standard aileron and ruddervator surfaces effective at trimming and control. They also allow a larger degree of control over the aircraft's dynamics through a wider range of flight conditions.

For the purposes of this initial study, the aircraft is modeled in the longitudinal plane only; that is, roll, yaw, and sideslip dynamics are not considered. By eliminating lateral dynamics, the number of parameters in the aerodynamic model is greatly reduced and asymmetric geometric configurations need not be considered. Also, it is assumed a priori that the optimal perching trajectory, in terms of curvilinear distance, time to land, or overall energy consumption, will be confined to the longitudinal plane. Even restricted to this plane, lateral dynamics enter into the model when considering poststall aerodynamics, which feature asymmetric flows and disturbance rejection from sideslip wind gusts; however, both of these phenomena are beyond the scope of this study.

In the present aerodynamic model, the fuselage and wings are modeled as a blended-wing body and the tail is considered as a separate lifting surface. The aerodynamic forces on the aircraft components are calculated using a modified version of Weissinger's method [6]. This analysis assumes that the wing quarter-chord line and chord distribution are expressed as an arbitrary function of the span; it is not restricted to straight-swept wings. However, this method assumes no sideslip, which is a reason why this analysis is restricted to the longitudinal plane only. Also, this theory assumes small angles of attack, thus high-angle of attack, separated flow is not considered here. The advantages of using an analytical method such as this are its speed and reconfigurability. It allows the computation of aerodynamic properties of nonconventional wing geometries, such as those of this perching aircraft, in a matter of minutes compared with the hours or days a computational fluid dynamics (CFD) analysis would require. Also, the quarter-chord curves, chord distributions, and twist distributions are input as piecewise analytical functions of the span coordinate, therefore, the wing geometry may be easily and quickly modified between aerodynamic analyses to account for aircraft reconfigurations.

This aerodynamic model of the aircraft is used to study the longitudinal dynamics of the vehicle and to simulate the perching maneuver. Specifically, the variation of the trim conditions as the shape morphs is discussed. The linearized dynamics around these trim points (the dynamic modes) are analyzed for stability using standard linear system analyses. Analyses of the cruise configuration as well as the initiation of the perching maneuver are presented, both within the range of validity of the aerodynamic model. The longitudinal dynamics of this shape change are simulated using a nonlinear three-degree-of-freedom aircraft simulation developed in the Simulink programming environment.

All dimensional results presented herein refer to a prototype of the ARES-C that was fabricated at Cornell in 2004. The aircraft's wingspan (tip to tip) is approximately 2 m and its weight is approximately 40 N.

Problem Formulation

To predict the dynamics of the ARES-C, first an accurate model of the aerodynamic forces is developed for various vehicle configurations and flight conditions. This model is an extended lifting-line model based off of Weissinger's method for straight, swept wings. This analysis method also incorporates real airfoil force data, which may be obtained from CFD programs or wind tunnel experiments. This is accomplished by following the reasoning of DeYoung and Harper [7], who suggest the method of distorting the chord length distribution along the wing such that the dimensional circulation about every span station matches the dimensional circulation of an ideal airfoil with the original chord length. This correction for real airfoils may alternatively be factored in by adjusting the wing incidence angle along the span.

To match closely the aerodynamics of the ARES craft, airfoils whose lift-to-drag characteristics resemble the ARES' airfoils [8] are selected for the ARES-C. This is accomplished by analyzing the ARES' airfoils using a CFD analysis, computed using Fluent, that simulates the Mars environment. A catalog of low-speed airfoil data, provided by the University of Illinois at Urbana-Champaign [9], is referenced in order to choose these airfoils. As with the ARES, three airfoils are chosen: one for the fuselage centerline, one for the wing root, and one for the wing tip. In between these span stations, the wing cross sections are lofted (i.e., interpolated) linearly. The lift data gathered for the three selected airfoils are presented in Fig. 3, and their span locations on the ARES-C are shown in Fig. 4.

This aerodynamic analysis is used to generate look-up tables for a longitudinal simulation of the ARES-C. Consequently, the simulation is only valid in the range of the airfoil data given in Fig. 3 and the moderate angle-of-attack regime of lifting-line theory.

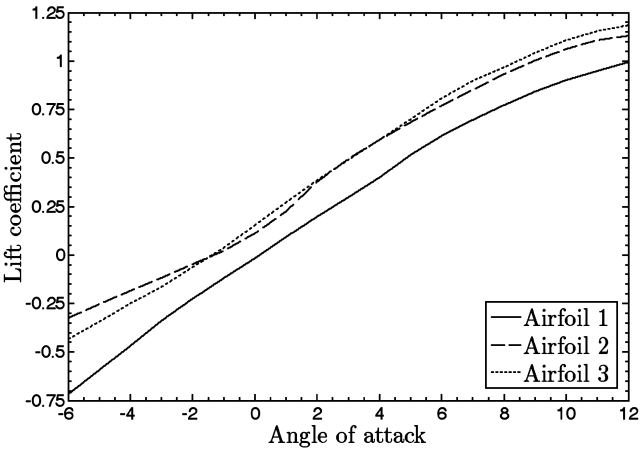

Fig. 3 Lift curves of ARES-C airfoils.

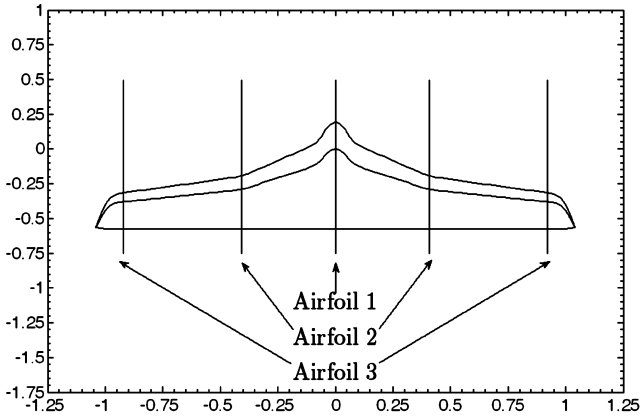

Fig. 4 ARES-C airfoil span locations.

The dynamics of the ARES-C are governed by the traditional equations of motion for aircraft:

$$\frac{\mathrm{d}m}{\mathrm{d}t}\mathbf{v} + m\frac{\mathrm{d}\mathbf{v}}{\mathrm{d}t} + \boldsymbol{\omega} \times m\mathbf{v} = \mathbf{f} + m\mathbf{T}\mathbf{g} \tag{1}$$

$$\frac{\mathrm{d}\mathbf{x}}{\mathrm{d}t} = \mathbf{T}^T\mathbf{v} \tag{2}$$

$$\frac{\mathrm{d}\mathbf{I}}{\mathrm{d}t}\boldsymbol{\omega} + \mathbf{I}\frac{\mathrm{d}\boldsymbol{\omega}}{\mathrm{d}t} + \boldsymbol{\omega} \times \mathbf{I}\boldsymbol{\omega} = \mathbf{m} \tag{3}$$

$$\dot{\mathbf{q}} = \frac{1}{2}\begin{bmatrix} 0 & -\boldsymbol{\omega} \\ \boldsymbol{\omega} & \boldsymbol{\omega}^{\times} \end{bmatrix}\mathbf{q} \tag{4}$$

Note the special consideration in Eq. (3) for a time-varying moment of inertia matrix. Also note that the forces and moments are given in local (noninertial) aircraft body coordinates so that aerodynamic data may be used from the lifting-line analysis. The subsequent analyses only consider the longitudinal dynamics, and so the side force, roll, and yaw equations are disregarded. Thus, the above set of 13 equations (Eqs. (1–4)), is reduced to the following set of six scalar equations:

$$\dot{u} = \frac{1}{m}(f_x - \dot{m}u) - wq - g\sin\theta \tag{5}$$

$$\dot{w} = \frac{1}{m}(f_z - \dot{m}w) + uq + g\cos\theta \tag{6}$$

$$\dot{x} = u\cos\theta + w\sin\theta \tag{7}$$

$$\dot{z} = -u\sin\theta + w\cos\theta \tag{8}$$

$$\dot{q} = \frac{1}{I_y}(m_y - \dot{I}_y q) \tag{9}$$

$$\dot{\theta} = q \tag{10}$$

To analyze the change in aircraft trim states under various flight conditions and geometrical configurations, the derivatives in the above equations of motion are zeroed, and the steady-state conditions are obtained as follows:

$$0 = m_y \tag{11}$$

$$0 = f_z + mg\cos\theta \tag{12}$$

$$0 = f_x - mg\sin\theta \tag{13}$$

Written in terms of aerodynamic forces and moments, these equations become

$$0 = M(\alpha, \delta_e, \delta_a, V) \tag{14}$$

$$0 = -D(\alpha, \delta_e, \delta_a, V)\sin\alpha - L(\alpha, \delta_e, \delta_a, V)\cos\alpha + mg\cos\theta \tag{15}$$

$$0 = -D(\alpha, \delta_e, \delta_a, V)\cos\alpha - L(\alpha, \delta_e, \delta_a, V)\sin\alpha - mg\sin\theta + T \tag{16}$$

where parameter dependence is noted for the lift, drag, and pitching moment terms. Other morphing parameters, such as wing incidence or tail boom angle, are not present; they are not considered to be dependent variables in trimming the aircraft. Note that symmetric ruddervator deflection is denoted δ_e here and throughout the rest of this article, because its use is synonymous with elevator deflection. The angle of attack and aileron deflection angle are fixed in order to calculate the trim condition at those angles. This will determine if the aircraft is "flyable"; that is, if it can be trimmed at every angle of attack during cruise. This will also allow the geometrical state of the aircraft to be treated as an independent variable, such that the dynamics of the aircraft can be described as functions of the morphing parameters. This system of nonlinear equations is triangular, meaning it can be solved sequentially in the order given. Although Eq. (14) still depends on both elevator deflection and velocity, the trim elevator position does not depend on the vehicle's velocity in the linear aerodynamic range, because in this regime changes in velocity scale the load distribution between the wings and tail uniformly. Subsequently, Eq. (15) can be solved for velocity and Eq. (16) can be solved for thrust.

To study the stability of these trim conditions as the flight condition and geometrical configuration change, the equations of motion are linearized about each trim point. This is accomplished through the usual Taylor Series expansion of the forces and moments, yielding the following linear system of longitudinal dynamics equations [10]:

$$\frac{\mathrm{d}}{\mathrm{d}t}\begin{pmatrix} u/V \\ \alpha \\ q \\ \theta \end{pmatrix} = \begin{bmatrix} X_u & \frac{X_\alpha}{V} & 0 & \frac{-g\cos\Theta_0}{V} \\ \frac{VZ_u}{V-Z_{\dot{\alpha}}} & \frac{Z_\alpha}{V-Z_{\dot{\alpha}}} & \frac{V+Z_q}{V-Z_{\dot{\alpha}}} & \frac{-g\sin\Theta_0}{V-Z_{\dot{\alpha}}} \\ VM_u + \frac{VZ_uM_{\dot{\alpha}}}{V-Z_{\dot{\alpha}}} & M_\alpha + \frac{VZ_uM_{\dot{\alpha}}}{V-Z_{\dot{\alpha}}} & M_q + \frac{(V+Z_q)M_{\dot{\alpha}}}{V-Z_{\dot{\alpha}}} & \frac{-M_{\dot{\alpha}}g\sin\Theta_0}{V-Z_{\dot{\alpha}}} \\ 0 & 0 & 1 & 0 \end{bmatrix} \times \begin{pmatrix} u/V \\ \alpha \\ q \\ \theta \end{pmatrix} + \begin{bmatrix} \frac{X_{\delta_e}}{V} \\ \frac{Z_{\delta_e}}{V-Z_{\dot{\alpha}}} \\ M_{\delta_e} + \frac{VZ_{\delta_e}M_{\dot{\alpha}}}{V-Z_{\dot{\alpha}}} \\ 0 \end{bmatrix}\delta_e \tag{17}$$

In Eq. (17), subscripted variables indicate with respect to which variable each force or moment is differentiated. Here, the derivatives $X_{(\cdot)}$ and $Z_{(\cdot)}$ are of the aircraft body forces f_x and f_z, respectively. The rotary derivatives $(\cdot)_u$ and acceleration derivatives $(\cdot)_{\dot{\alpha}}$ are estimated using empirical relations given in the USAF Data Compendium (Datcom) [11] based on the static data computed with the aforementioned lifting-line method. For each trim condition, a new plant matrix given by Eq. (17) is computed using the aerodynamic look-up tables and Datcom methods. The dynamic mode shapes and natural frequencies can then be computed straightforwardly from the plant matrix.

A Simulink model of the dynamics of the perching aircraft is developed to simulate the trajectory of the aircraft as it morphs from a

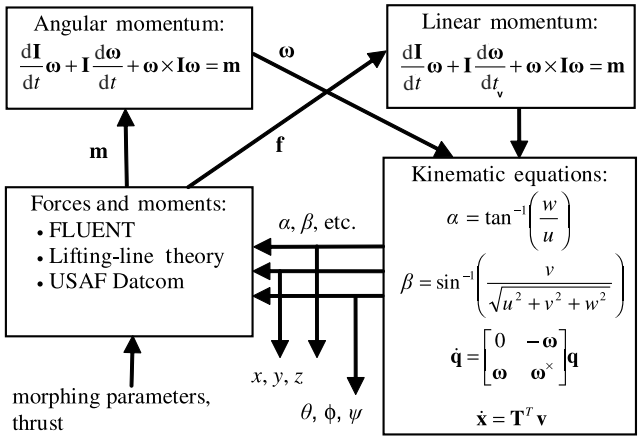

Fig. 5 Overview of morphing aircraft simulator.

cruise configuration to the initiation of the perching maneuver. This model is designed to be expandable and modular so that various morphing vehicles or sets of aerodynamic data may be run in the same simulator. A schematic of this simulator appears in Fig. 5, based off of a standard six-degree-of-freedom simulation [12].

This diagram shows the cyclical nature of the simulation process. Morphing parameters, such as wing incidence angle and tail boom angle, are the generalized inputs to this system, augmenting traditional inputs such as elevator or rudder deflections. The aforementioned lifting-line theory and Datcom methods are used to determine the aerodynamic forces and moments on the aircraft at each step during its flight based on the current flight condition and vehicle configuration. These forces and moments determine the change in aerodynamic state for the next iteration. This model uses the quaternion representation for the heading angles and a 4th–5th order Runge–Kutta method for the numerical integration.

Results

To simulate how the aircraft morphs through various shape configurations and flight conditions, a look-up table of the aerodynamic loads in terms of every varying parameter is constructed. These parameters are listed in Table 1 and are defined in Fig. 6. The speed and reconfigurability of the aforementioned lifting-line theory are used in the construction of this table; the over 9500 combinations of geometry and flight conditions used in the simulation can be tabulated in a matter of days. Some results of this analysis on the tail are presented in Fig. 7 and the results from the blended-wing body are presented in Fig. 8. Figures 7a and 7b show the variation of the tail loads as a function of angle of attack and symmetric ruddervator deflection. These plots show that the ruddervators start to lose their effectiveness at high deflections and angles of attack due to flow separation introduced by the experimental airfoil data. Also note in Fig. 7b that there is very little difference between tail incidence and ruddervator deflection because the ruddervators comprise about 75% of the tail's planform area. Figures 8a and 8b depict the variation of aerodynamic loads on the fuselage blended-wing body as the angle of attack and wing incidence angle change. This analysis predicts that drag increases and lift decreases uniformly as the negative wing incidence increases, as expected. Also, the minimum drag increases significantly as the wings are rotated because at no point is the entire blended-wing body at the angle of attack for minimum drag. Thus, this geometrical change is shown to be effective in the initiation of the perching maneuver.

This look-up table of aerodynamic data is used in the longitudinal dynamics simulation and analysis of the ARES-C. To determine the flight-worthiness of the aircraft, it is desired to trim the craft at every point within the linear range of angles of attack, with or without use of symmetric aileron deflection. These results for various angles of attack and symmetric aileron (i.e., flaperon) deflections are presented in Fig. 9. These plots indicate that the ARES-C follows the trends of standard aircraft. More ruddervator deflection is needed to trim at

Table 1 Parameter variations in aerodynamic database

α	angle of attack	−5 deg –15 deg
ι	wing incidence angle	−15 deg –0 deg
θ_b	tail boom angle	−15 deg –45 deg
θ_t	tail incidence angle	−5 deg –15 deg
δ_a	symmetric aileron deflection angle	−20 deg –20 deg
δ_e	symmetric ruddervator deflection angle	−20 deg –20 deg

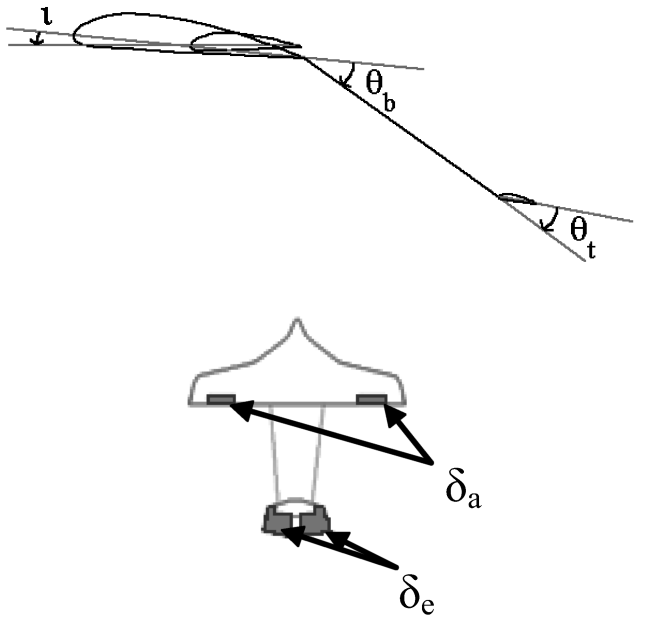

Fig. 6 ARES-C morphing parameters.

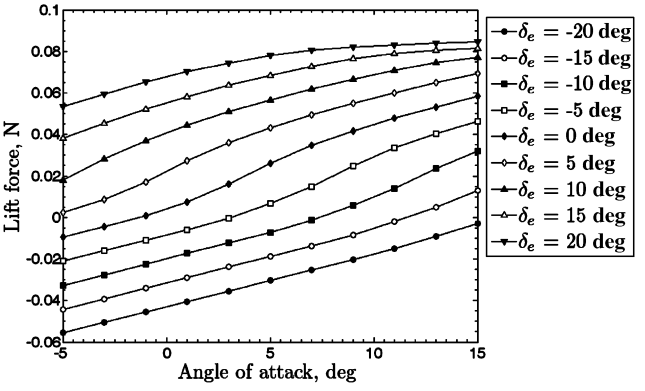

a)

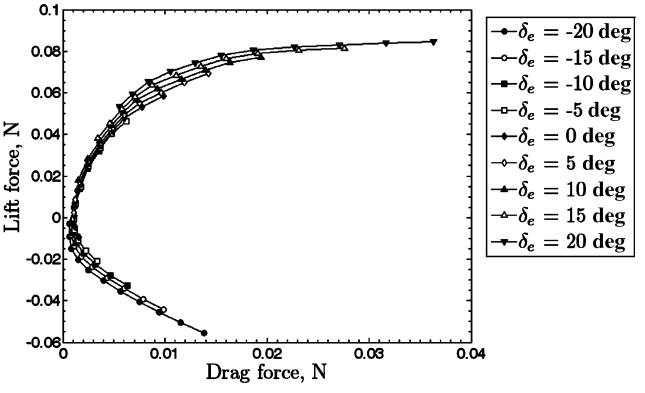

b)

Fig. 7 Aerodynamic data on the tail calculated by the modified Weissinger's method.

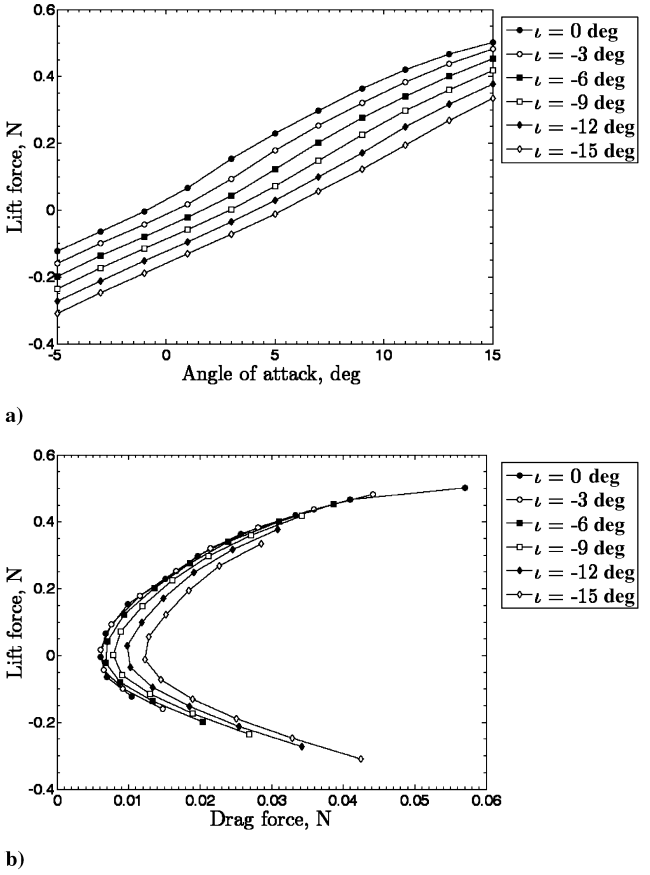

Fig. 8 Aerodynamic data on the blended-wing body calculated by the modified Weissinger's method.

higher angles of attack and minor flaperon deflection is needed to trim at negative angles of attack through adding slight camber to the wings. Naturally, the trim velocity decreases as angle of attack increases due to increased lift generation by the wings and fuselage. Finally, the trim thrust has a minimum around 3–4 deg angle of attack for positive flaperon deflections. All conditions correspond to a trim thrust-to-weight ratio of around 1/10. The angle of attack for minimum power occurs between 7–9 deg, with the higher angles corresponding to lower trim flaperon deflections. In terms of performance, the minimum thrust corresponds to the maximum range, whereas the minimum power corresponds to the maximum endurance.

The stability of each trim condition is analyzed by plotting the migration of the eigenvalues of the plant matrix given by Eq. (17). The entries of this matrix are recomputed for each flight condition using a combination of table lookups and Datcom formulas. Figure 10 shows the migration of the aircraft's longitudinal eigenvalues as angle of attack varies from −3–10 deg. For most trim conditions, there are two pairs of complex conjugate eigenvalues corresponding to the short-period and phugoid modes of pitch oscillation. The short-period mode can be described as a rapid, highly damped pitch oscillation, whereas the phugoid mode is a long-period, lightly damped porpoising mode with very little angle-of-attack variation. As shown, the short-period mode becomes less stable at higher angles of attack due to decreased effectiveness of the tail at creating restoring moments. At negative angles of attack, these oscillations disappear. One of the overdamped modes approaches instability due to the decrease in restoring moment by the wings.

The variation of the longitudinal dynamics as the perching maneuver is initialized is also examined. This maneuver consists of a wing incidence rotation by 5 deg and a rotation of the tail boom downward by 60 deg, as shown in Fig. 11a. This maneuver is compared with a standard speed reduction through pitching up the nose with no geometrical reconfiguration, as shown in Fig. 11b. Both

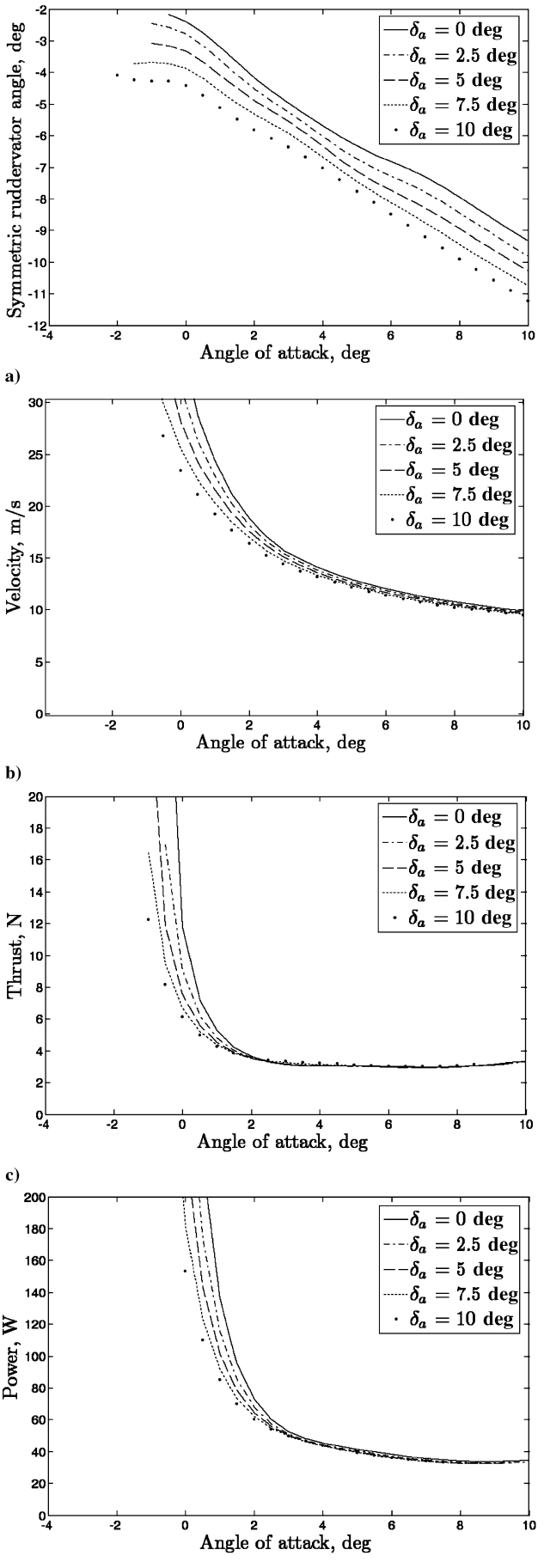

Fig. 9 Trim results for various angles of attack and symmetric aileron (flaperon) deflections.

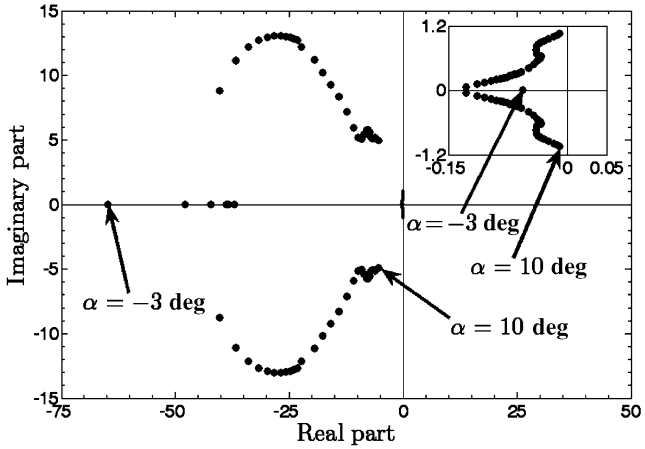

Fig. 10 Eigenvalue migration as trim angle of attack varies ($\delta_a = 5$ deg).

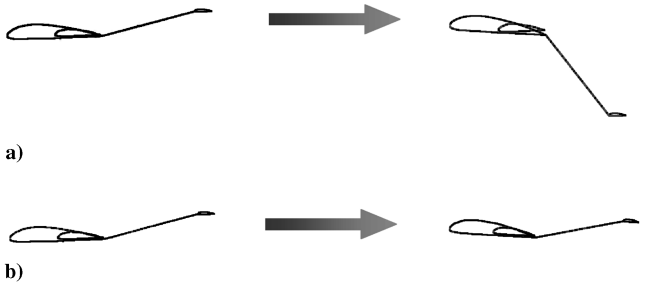

Fig. 11 Maneuvers for comparison: a) initiation of perching, and b) pitch-up.

of these maneuvers result in an increase in the fuselage angel of attack from 0 to 5 deg. Figure 12 depicts the change in trim condition (symmetric ruddervator deflection, velocity, and thrust) throughout the maneuvers. Figure 12 indicates that both maneuvers result in a reduction in cruise velocity and thrust with the reduction resulting from the pitch-up being greater than the perching maneuver. However, the trim deflection of the ruddervator is much greater in the pitch-up case, meaning that it becomes less useful in trimming and controlling the aircraft at higher pitch angles. This example highlights one of the advantages of vehicle reconfiguration; the control surfaces remain highly effective under various flight conditions. Here, the trim position of the ruddervators remains relatively unchanged as the vehicle's angle of attack increases. The short-period mode is affected the greatest during these maneuvers; the natural frequency of this mode is decreased in both cases due to the reduction in tail effectiveness at high angles of attack. In both cases, the eigenvalues approximately move along lines of constant damping. Damping is reduced during the initiation of the perching maneuver due to the reduction in the tail moment arm during the rotation of the tail boom. The differences in eigenvalue migrations seen in Fig. 13 can, therefore, be most attributed to the manipulation of center of pressure, and to a lesser extent, center of gravity, that the geometrical reconfiguration of the perching maneuver accomplishes.

To simulate these maneuvers, it is assumed that the aircraft passes through a series of quasi-static trim conditions as the geometry morphs. These conditions are calculated using the previously described trim analysis. The morphing parameters and control deflections needed for each trim condition are then fed into the simulation as commanded inputs. Since the dynamics are nonlinear, there is no guarantee that the dynamic response will be stable; however, if the maneuver is performed slowly enough, excursions away from the trim points are minimized. The resulting trajectories for the perch and the pitch-up maneuvers are shown in Fig. 14.

In these cases, the maneuvers last from $t = 10$s until $t = 30$s. Note that these maneuvers produce stable responses with relatively small

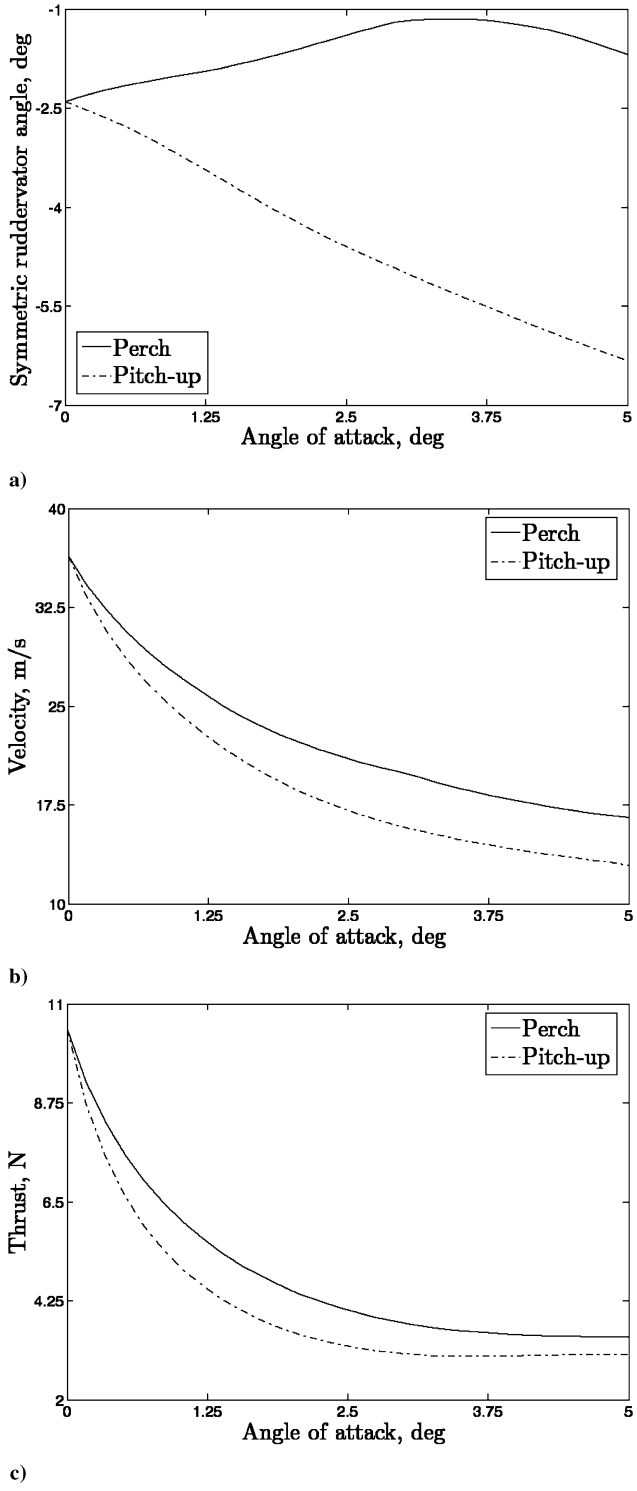

Fig. 12 Change in trim conditions throughout the maneuvers.

changes in steady-state altitude (compared to the distance traveled). Both the phugoid and short-period modes are excited, although only the phugoid mode is evident in Figs. 14–16. The angle of attack reaches a peak at 5.5 deg for the perching maneuver and 8 deg for the pitch-up, with a steady-state value of 5 deg for both cases (thus returning the wings to a 0 deg angle of attack for the perching case). As depicted in Fig. 12b, both maneuvers reduce the trim velocity of the vehicle, with the pitch-up maneuver reducing it further. In addition, the pitch-up response is more highly damped; the only drawbacks are the increased overshoot in the transient response and the increased ruddervator deflection as discussed in the preceding section.

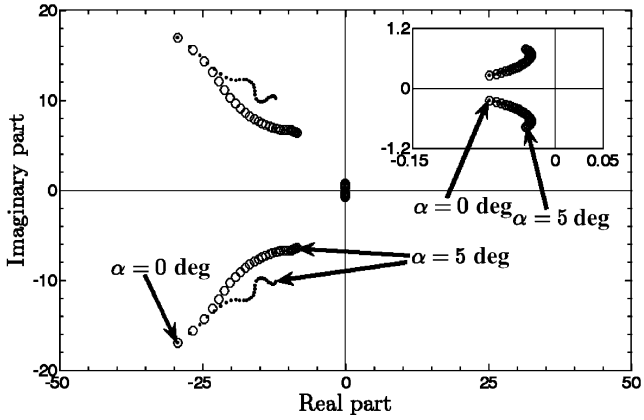

Fig. 13 Eigenvalue migration throughout the maneuvers: the initiation of perching (∘) and pitch-up (·).

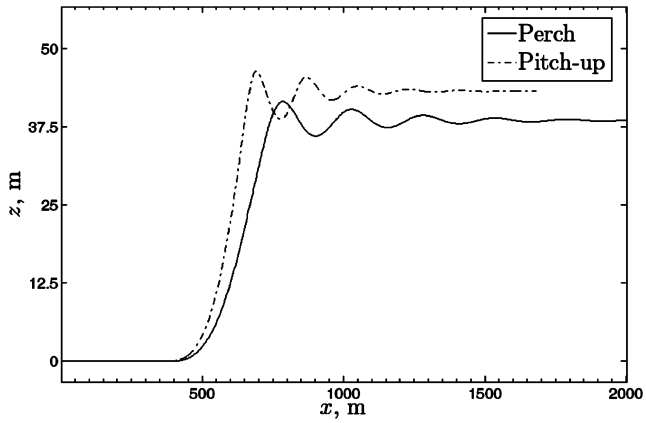

Fig. 14 Open-loop position responses to commanded maneuvers.

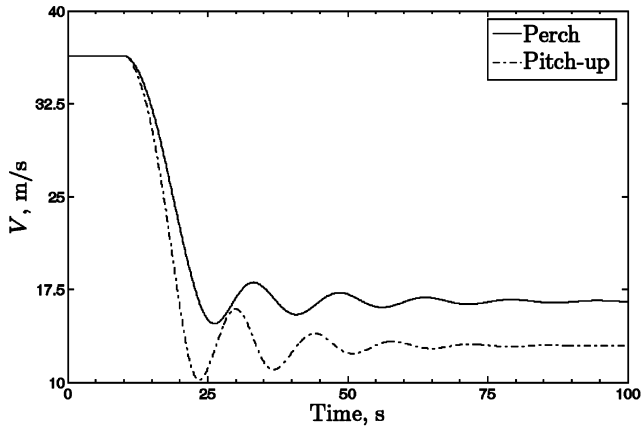

Fig. 15 Open-loop velocity responses to commanded maneuvers.

Conclusion

The transient and steady-state behavior of a perching aircraft undergoing changes in flight condition and vehicle reconfiguration is discussed. This aircraft's unique morphology (consisting of variable wing incidence, tail boom angle, and tail incidence) is presented and shown to be effective for the initiation of a perching maneuver. The perching shape reconfiguration and a simple pitch-up are compared at low angles of attack using analytical and empirical methods. Whereas the pitch-up maneuver permits a similar reduction in air speed, vehicle reconfiguration avoids large steady-state deflections of the longitudinal control surfaces. Simulations also show that, although the pitch-up is more highly damped, its transient behavior brings the aircraft closer to instability at high angles of attack.

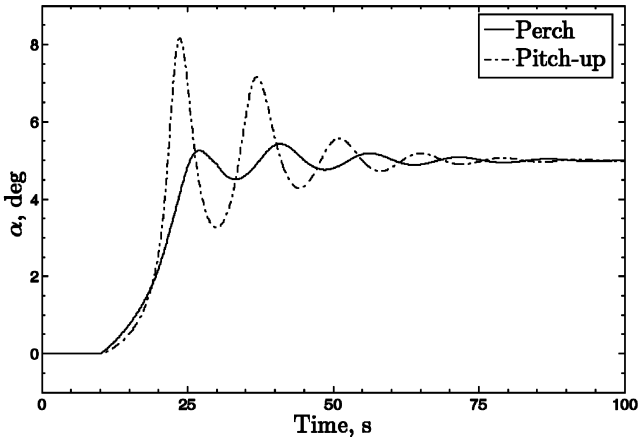

Fig. 16 Open-loop angle-of-attack responses to commanded maneuvers.

Although simulation at low angles of attack does not suggest any new capabilities enabled by shape reconfiguration, at poststall angles of attack reconfiguration will be necessary to trim the aircraft because attached flow will still be present over the wings and tail surfaces.

Acknowledgment

This work is supported by the NASA Langley Research Center through the Graduate Student Research Program; grant number NGT-1-03022. This grant is monitored by Martin Waszak and Anna-Maria McGowan.

References

[1] Sanders, B., Crowe, R., and Garcia, E., "Defense Advanced Research Projects Agency: Smart Materials and Structures Demonstration Program Overview," *Journal of Intelligent Material Systems and Structures*, Vol. 15, No. 4, 2004, 227–233.

[2] Bowman, J., Sanders, B., and Weisshaar, T., "Evaluating the Impact of Morphing Technologies on Aircraft Performance," AIAA2002-1631, 2002.

[3] Wickenheiser, A., Garcia, E., and Waszak, M., "Evaluation of Bio-Inspired Morphing Concepts with Regard to Aircraft Dynamics and Performance," *Proceedings of SPIE: International Society for Optical Engineering*, Vol. 5390, 2004, pp. 202–211.

[4] Wickenheiser, A., Garcia, E., and Waszak, M., "Longitudinal Dynamics of a Perching Aircraft Concept," *Proceedings of SPIE: International Society for Optical Engineering*, Vol. 5764, 2005, pp. 192–202.

[5] Levine, J. S., Blaney, D. L., Connerney, J. E. P., Greeley, R., Head, J. W., Hoffman, J. H., Jakosky, B. M., McKay, C. P., Sotin, C., and Summers, M. E., "Science from a Mars Airplane: The Aerial Regional-Scale Environmental Survey (ARES) of Mars," AIAA2003-6576, 2003.

[6] Weissinger, J., "The Lift Distribution of Swept-Back Wings," NACA, TM-1120, 1947.

[7] DeYoung, J., and Harper, C. W., "Theoretical Symmetric Span Loading at Subsonic Speeds for Wings Having Arbitrary Plan Form," NACA, Report No. 921, 1948.

[8] Smith, S. C., Guynn, M. D., Streett, C. L., and Beeler, G. B., "Mars Airplane Airfoil Design with Application to ARES," AIAA2003-6607, 2003.

[9] McGranahan, B., and Selig, M., *UIUC Low-Speed Airfoil Tests*, URL: http://www.aae.uiuc.edu/m-selig/uiuc_lsat.html [cited 19 Feb. 2004].

[10] Schmidt, L., *Introduction to Aircraft Flight Dynamics*, AIAA Education Series, AIAA, Reston, VA, 1998, p. 113.

[11] Hoak, D. E., and Finck, R. D., "The USAF Stability and Control Datcom," Air Force Wright Aeronautical Lab., TR-83-3048, Oct. 1960 (Revised 1978).

[12] Zipfel, P., *Modeling and Simulation of Aerospace Vehicle Dynamics*, AIAA Education Series, AIAA, Reston, Virginia, 2000, p. 378.

[13] Qualls, G., *ARES: A Proposed Mars Scout Mission*, URL: http://marsairplane.larc.nasa.gov/multimedia.html [cited 10 Feb. 2004].

R. Duffy
Associate Editor